Journal of Computational Physics 387 (2019) 117–133

Contents lists available at ScienceDirect

Journal of Computational Physics

www.elsevier.com/locate/jcp

Adaptive numerical homogenization for upscaling single phase flow and transport

Yerlan Amanbek [a,c,*], Gurpreet Singh [a], Mary F. Wheeler [a], Hans van Duijn [b]

[a] Center for Subsurface Modeling, Institute for Computational Engineering and Sciences, University of Texas at Austin, 201 East 24th St, Stop C0200, POB 4.102, Austin, TX, USA
[b] Technische Universiteit Eindhoven, P.O. Box 513, 5600 MB Eindhoven, Netherlands
[c] Nazarbayev University, Kabanbay Batyr Avenue 53, Astana, Kazakhstan

ARTICLE INFO

Article history:
Received 31 December 2017
Received in revised form 10 December 2018
Accepted 14 February 2019
Available online 5 March 2019

Keywords:
Enhanced velocity
Numerical homogenization
Adaptive mesh refinement
Multiscale methods

ABSTRACT

We propose an adaptive multiscale method to improve the efficiency and the accuracy of numerical computations by combining numerical homogenization and domain decomposition for modeling flow and transport. Our approach focuses on minimizing the use of fine scale properties associated with advection and diffusion/dispersion. Here a fine scale flow and transport problem is solved in subdomains defined by a transient region where spatial changes in transported species concentrations are large while a coarse scale problem is solved in the remaining subdomains. Away from the transient region, effective macroscopic properties are obtained using local numerical homogenization. An Enhanced Velocity Mixed Finite Element Method (EVMFEM) as a domain decomposition scheme is used to couple these coarse and fine subdomains [1]. Specifically, homogenization is employed here only when coarse and fine scale problems can be decoupled to extract temporal invariants in the form of effective parameters. In this paper, a number of numerical tests are presented for demonstrating the capabilities of this adaptive numerical homogenization approach in upscaling flow and transport in heterogeneous porous medium.

1. Introduction

Accurate modeling of flow and transport is important in evaluating oil and gas recovery, nuclear waste disposal systems, CO_2 sequestration, and groundwater remediation in subsurface porous media. Efficient numerical modeling of the associated physical processes has several challenges due to the heterogeneity, the uncertainty and the multiscale nature of porous media parameters. The main source of obtaining these parameters is borehole measurements which are sparsely distributed in space. Reservoir parameters are populated using these measurements in conjunction with geostatistical methods including parameter estimation and uncertainty quantification. For a given scenario, however, a direct numerical simulation of the flow and transport problem based on these fine scale parameters is often computationally prohibitive. Additionally, the datasets obtained from different observation sources may vary strongly in characteristic spatial scales. For example, borehole and seismic measurements have a resolution varying between a few feet to hundreds of feet, respectively. A coarse scale numerical model, which can handle multiple Representative Elementary Volumes (REV), is therefore necessary to reduce computational overheads associated with solving a fine scale problem. However, ad-hoc averaging techniques may fail to

* Corresponding author at: Nazarbayev University, Kabanbay Batyr Avenue 53, Astana, Kazakhstan.
E-mail address: yerlan@utexas.edu (Y. Amanbek).

https://doi.org/10.1016/j.jcp.2019.02.014

capture fine scale features resulting in a loss of numerical accuracy that compromises the predictive nature of the model. Thus, development of mathematically consistent upscaling techniques is necessary for preserving solution accuracy for field scale problems.

The multiscale nature of flow and transport problems in porous medium has been addressed in [2–7] giving rise to a number of approaches for upscaling. Each of these schemes performs computations at a coarse scale aiming to capture fine scale physics as close as possible. However, upscaling tends to reduce the fine scale property information either by averaging or by identifying a reduced number of characteristic parameters. We briefly discuss two widely used upscaling techniques, homogenization and multiscale bases.

Homogenization theory is a well-established and mathematically consistent, theoretical framework for understanding the multiscale nature of subsurface problems. Earlier studies by [8–12] use homogenization theory for upscaling rapidly oscillating model parameters. These parameters include rock properties such as permeability, porosity, dispersion as well as model parameters for relative permeability and heterogeneous chemical reactions. The two-scale homogenization theory relies upon the assumption of an identifiable period (or REV) in an otherwise heterogeneous medium with a characteristic length scale much smaller than the length scale of the medium under investigation. In other words, the ratio of the length of the period to the medium, denoted by ε, is sufficiently small. This assumption leads to a scale separation between fine and coarse scale problems thereby decoupling the computations associated with each of the two problems. Given fine scale parameters the effective properties at the coarse scale can then be evaluated following two-scale homogenization theory in the limit of $\varepsilon \to 0$. In [13,14], the well-known Darcy law is derived from Stokes (Navier-Stokes) equation at the pore scale.

In numerical simulations a small value of ε is employed. However, the requirements of periodicity and scale separation are often too restrictive for direct application to realistic, heterogeneous, porous medium problems. Nevertheless, homogenization is an indispensable mathematical tool in providing valuable insight into the multiscale nature of porous media problems by describing coarse scale parameters as functions of fine scale variations. In Section 3, we describe how adaptivity can relax the scale separation and periodicity assumptions for flow and particularly transport problems.

A number of multiscale methods have been proposed for a wide range of problems. Although incomplete, we provide a brief literature description of several well-known approaches. Multiscale finite element methods (MsFEM) were introduced by Babuška et al. [15] in the framework of the generalized finite element method (GFEM) for elliptic problems with rough coefficients. Here, the multiscale basis functions were obtained by solving local problems with appropriate boundary conditions and vanishing right hand sides. This idea was later extended to general heterogeneities by Hou and Wu in [16] using oversampling techniques to obtain improved accuracy. Further extensions [17,18] involved the development of the Generalized Multiscale Finite Element Method (GMsFEM). This framework systematically enriches the coarse solutions by modifying the multiscale basis functions dynamically. A similar but locally mass conservative approach is the multiscale finite-volume method (MsFVM) [19–22]. These latter works rely upon effective transmissibility computations on a primal coarse grid by solving fine scale subdomain problems with boundary conditions obtained from a dual coarse grid solution.

The variational multiscale methods (VMS) introduced by Hughes et al. [23] decomposes the solution space into fine and coarse scale parts. This method combines dominant coarse and fine scale effects in the form of a stabilized variational problem to represent the coarse scale solution. Based on VMS a locally conservative mixed finite element, multiscale method was also presented by Arbogast et al. [4,24]. Another well-known multiscale scheme is the heterogeneous multiscale method (HMM), which has been applied to a number of multiphysics problems [25–27]. This method couples the macroscopic and microscopic models by assuming a scale separation similar to two-scale homogenization theory. Multiscale Mortar Mixed FEM (MM MFEM) is another approach for coupling multiscale and multiphysics subdomains through specialized interface conditions, where continuity conditions were imposed across different scales [28–33]. The mortar method had been used to improve solution accuracy of heterogeneous problems by adaptively enriching the multiscale mortar space.

In this work, we investigate local numerical homogenization for upscaling coupled flow and transport in porous medium. We obtain computational efficiency while maintaining solution accuracy by combining a local homogenization with an Enhanced Velocity Mixed Finite Element Method (EVMFEM) domain decomposition approach [1]. A fine scale problem is solved dynamically in subdomains defined by transient regions while a coarse scale problem is solved over remaining subdomains. The transient regions are identified by sharp fronts associated with species transport. In this aspect, our method shares similarities with the adaptive [34,35] multiscale methods, where a coarse problem is enriched locally to capture fine scale physical features. Away from the transient region, effective properties of macroscopic equations at the coarse scale are obtained using local numerical homogenization. Our method is locally mass conservative at both coarse and fine scales. The adaptivity allows us to circumvent expensive computations of effective dispersion tensor using local numerical homogenization.

This paper is organized as follows: Section 2 describes the coupled flow and transport model formulation, Section 3 provides a brief summary of effective macroscale equations using two-scale homogenization theory followed by a description of the EVMFEM adaptive mesh refinement (AMR) approach. The details of our proposed adaptive numerical homogenization scheme are then presented in Section 4. Numerical results in Section 5 demonstrate the feasibility of our scheme using realistic SPE10 datasets [36]. Finally, Section 6 summarizes and concludes our work.

2. Model formulation

We begin by describing the flow and transport model formulation along with initial and boundary conditions. We consider a single phase, slightly compressible fluid in porous medium with a non-reactive species transport. The phase mass conservation equation on a domain Ω is given by,

$$\frac{\partial}{\partial t}(\phi\rho) + \nabla\cdot(\rho\mathbf{u}) = q \qquad \text{in} \quad \Omega\times J \tag{1}$$

Here, $\Omega\in\mathbb{R}^d (d=1,2 \text{ or } 3)$, $J=(0,T]$, d is the number of spatial dimensions, q is the source/sink term, ϕ is the porosity, ρ is the phase density, and $\mathbf{u}$ is the phase velocity. We remark that a Peacemann correction is used for modeling source/sink terms [37]. The slightly compressible fluid density is defined as a function of pressure as follows,

$$\rho = \rho_{ref} e^{C_f(p-p_{ref})} \tag{2}$$

where, C_f is the fluid compressibility, and ρ_{ref} is the reference density at reference pressure p_{ref}. The phase velocity $\mathbf{u}$ is given by the Darcy's law as,

$$\mathbf{u} = -\frac{\mathbf{K}}{\mu}(\nabla p - \rho\mathbf{g}), \tag{3}$$

where, μ is the viscosity, $\mathbf{K}$ is the permeability (absolute permeability) tensor, ρ is the density of the fluid and $\mathbf{g}$ is the gravity vector. The conservation equation of a component i in the flowing phase is given by,

$$\frac{\partial}{\partial t}(\phi c_i\rho) + \nabla\cdot(c_i\rho\mathbf{u} - \phi\rho\mathbf{D}_i\nabla c_i) = q\hat{c}_i, \tag{4}$$

where, c_i and $\mathbf{D}_i$ are the normalized concentration and the positive definite, diagonal diffusion/dispersion tensor, respectively of component i in the flowing phase, and $\hat{c}_i$ is the injection/production concentration of the component i. We define diffusive flux $\mathbf{d}_i$ for a component i as,

$$\mathbf{d}_i = \phi\mathbf{D}_i\nabla c_i. \tag{5}$$

The concentrations c_i are constrained by,

$$\sum_{i=1}^{N_c} c_i = 1. \tag{6}$$

Although more general global boundary conditions can also be treated, we restrict ourselves to the following,

$$\begin{aligned} p &= g \quad \text{on} \quad \partial\Omega\times J, \text{ and} \\ \mathbf{D}_i\nabla c_i\cdot\boldsymbol{\nu} &= 0 \quad \text{on} \quad \partial\Omega\times J, \end{aligned} \tag{7}$$

where $\boldsymbol{\nu}$ is the unit outward normal. Additionally, the initial condition is given by,

$$\begin{aligned} p(x,0) &= p^0(x) \\ c_i(x,0) &= c_i^0(x) \quad \text{at} \quad \Omega\times\{0\}. \end{aligned} \tag{8}$$

3. Methodology

In this work, we apply a local numerical homogenization scheme motivated by two-scale homogenization theory to obtain effective equations at the coarse scale starting from fine scale mass conservation equations and constitutive relationship (Darcy's law). Once the coefficients for the coarse scale equations have been evaluated, we apply a EVMFEM domain decomposition approach to couple coarse and fine subdomains.

3.1. Two-scale homogenization

We inherit the definition of $\varepsilon = l/L$ from two-scale homogenization theory where l and L are the fine and coarse length scales. The assumption of scale separation (or $\varepsilon\to 0$) is a theoretical requirement for two-scale homogenization. The scale separation assumption here inherently implies that the pressure, velocity and species concentration unknowns vary slowly (relatively non-oscillatory) at the coarse scale compared to faster variations (or highly oscillatory) at the fine scale. Under the aforementioned two-scale ansatz the unknowns in pressure, velocity, density and concentration are formally expanded as power series in ε as,

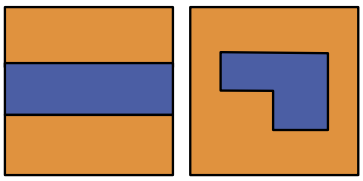

Fig. 3.1. Schematic of REVs for layered (left) and general (right) permeability distribution.

$$a_\varepsilon(x) = a_0(x, y) + \varepsilon a_1(x, y) + \varepsilon^2 a_2(x, y) + ... \tag{9}$$

Here, a can be any one of the primary unknowns pressure (p), velocity ($\mathbf{u}$), density (ρ) or species concentration (c). Further, x and y represent the coarse and fine scales such that $y = \frac{x}{\varepsilon}$ where $a(x, y)$ is used to denote the variations in an unknown at both the scales.

3.1.1. Flow

We apply the two-scale homogenization theory to single phase slightly compressible flow problem in order to derive the effective flow equations at the coarse scale. The parameters permeability and porosity are assumed to be oscillatory (or heterogeneous) parameters at the fine scale. The flow equations for slightly compressible flow at the fine scale have the following form

$$\begin{aligned} \mathbf{u}_\varepsilon &= -\mathbf{K}\left(\frac{x}{\varepsilon}\right)\nabla p_\varepsilon && \text{in } \Omega \\ \frac{\partial}{\partial t}(\phi\rho_\varepsilon) + \operatorname{div}(\rho_\varepsilon \mathbf{u}_\varepsilon) &= f && \text{in } \Omega \\ p &= g && \text{on } \partial\Omega \end{aligned} \tag{10}$$

where, ε denotes the two-scale variations in the unknowns $a_\varepsilon = a(x, y)$, $f \in L^2(\Omega)$ the source/sink term, and $\mathbf{K}$ and ϕ are the oscillatory (or heterogeneous) absolute permeability (symmetric, positive definite tensor) and porosity, respectively with period of oscillation $y = \frac{x}{\varepsilon}$, and $x, y \in \mathbb{R}^d$, $d = 1, 2, 3$.

Using the formal expansion (Eqn. (9)) in the unknowns and substituting in the system of Eqns. (10) we can obtain the effective macroscale equations following the derivation in [12] as follows,

$$\begin{aligned} \tilde{\mathbf{u}} &= -\mathbf{K}^{eff}\nabla p_0 && \text{in } \Omega \\ \frac{\partial}{\partial t}(\rho_0\langle\phi\rangle) + \operatorname{div}_x(\rho_0\tilde{\mathbf{u}}) &= f && \text{in } \Omega \\ p_0 &= g && \text{on } \partial\Omega \end{aligned} \tag{11}$$

where $\langle\phi\rangle = \int_Y \phi dy$, $\tilde{\mathbf{u}} = \int_Y \mathbf{u}_0 dy$, $\mathbf{K}^{eff}$ is a symmetric, positive definite tensor denoting the effective permeability at the coarse scale. Note that the effective permeability does not depend on the choice of the domain Ω, source term f, and boundary conditions on $\partial\Omega$. Furthermore, the eigenvalues of the effective permeability tensor are bounded below and above by harmonic and arithmetic means of eigenvalues, respectively of the fine scale permeability tensors. Arbogast [3] shows that the homogenized equations for the elliptic boundary value problem is well-posed which can be extended to the parabolic initial and boundary value problem discussed above. The effective permeability tensor is constructed using the solution (χ^i) of the auxiliary problem or a unit-cell problem for a dimensionless form of the above equations, on a periodic domain Y as follows;

$$\begin{aligned} -\nabla\cdot\left(\mathbf{K}(y)\left(\nabla\chi^i + e_i\right)\right) = 0 \quad \text{in } Y, \\ \chi^i \text{ is perodic in } Y. \end{aligned} \tag{12}$$

Here, $\{e_i\}_{1\le i\le d} \in \mathbb{R}^d$ is the canonical basis for a finite dimensional problem of dimension d.

An analytical derivation of effective permeability, using two-scale homogenization, for layered permeability distribution, with diagonal permeability tensor, is presented in [38]. This derivation results in the well-known arithmetic and harmonic averaging for flow along and across the layered medium, respectively. However, in order to use this result the REV must be chosen carefully so that the layered medium assumption and hence the aforementioned averaging applies. Fig. 3.1 shows REV for layered and general distribution of permeability. One must note that it is not always possible to select an REV which satisfies the layered distribution wherein a more general approach such as adaptive numerical homogenization becomes indispensable.

3.1.2. Transport

In this section, we briefly discuss the derivation of the effective equations at the macroscopic scale for slightly compressible flow similar to [12]. Although the effective macro-diffusion is not used in the present work, this discourse provides us insight into identification of invariants that can be used to reduce the computational costs in future works. We discuss the details of the computational costs and invariants in Subsection 4.3. It is important to note that, in this respect homogenization theory guides us towards development of adaptive solution algorithms to reduce the computational costs while preserving features/quantities of interest of a physical process.

A similar discourse, as discussed in Sub-section 3.1.1, is applied to the advection and diffusion problem Eqn. (4) to obtain the effective equations at the macroscopic scale described below. Here we briefly discuss the derivation of these equations; following the original work for incompressible flow in [12], for the sake of completeness. Since $\rho_0 = \rho_0(x)$ or the ϵ^0 order density varies only at the coarse scale, the derivation of effective transport equations for slightly compressible flow remains unchanged from the original derivation for incompressible flow. We define $\varepsilon = l/L$, $Pe = u^0 l/D^0$, $t_c = \phi^0 L/u^0$ and denote u^0, D^0, K^0, ρ_0 and ϕ^0 as characteristic Darcy velocity, diffusivity, permeability and rock porosity respectively. Based on this setting we introduce dimensionless space variable $x \mapsto x/L$, the dimensionless characteristic convection time $t \mapsto t/t_c$. Here, we assume scale separation, $\varepsilon \ll 1$ and large Peclet number $Pe = O(1)$; namely the fine scale transport is advection dominated. For more details see [12].

The dimensionless form of the transport equation is given by,

$$\begin{aligned} \phi\left(\frac{x}{\varepsilon}\right)\frac{\partial\left(\rho_\varepsilon c_\varepsilon\right)}{\partial t} + \mathbf{u}^\varepsilon \cdot \nabla\left(\rho_\varepsilon c_\varepsilon\right) = \frac{\varepsilon}{Pe}\nabla\cdot\left(\rho_\varepsilon \mathbf{D}\left(\frac{x}{\varepsilon}\right)\nabla c^\varepsilon\right) \quad &\text{on} \quad \Omega\times J, \\ c_\varepsilon(x,0) = c^0(x) \quad &\text{on} \quad \Omega\times\{0\}. \end{aligned} \tag{13}$$

Using the two-scale ansatz for c_ε, ρ_ε and $\mathbf{u}_\varepsilon$ as formulated in Eqn. (9). Similarly the homogenized equation; for ϵ^1 order accuracy in species concentration, is given by,

$$\langle\phi\rangle\frac{\partial\left(\rho_\varepsilon^1 c_\varepsilon^1\right)}{\partial t} + \langle\mathbf{u}_0\rangle\cdot\nabla_x\left(\rho_\varepsilon^1 c_\varepsilon^1\right) = \frac{\varepsilon}{Pe}\mathrm{div}_x\left(\rho_\varepsilon^1 \mathbb{D}^{eff}\nabla_x c_\varepsilon^1\right). \tag{14}$$

where, c_ε^1 and ρ_ε^1 are the macroscale species concentration. In addition, $\mathbb{D}^{eff}$ is the effective diffusivity tensor computed by solving another auxiliary problem. Further, $\langle\phi\rangle$ is the volume averaged porosity and $\langle\mathbf{u}_0\rangle$ is the effective (or coarse) Darcy velocity. As in [12], we obtain the effective diffusivity for each $x\in\Omega$

$$\mathbb{D}^{eff}(x) = \mathcal{D}^h\left(Pe\nabla p_0(x)\right) + \mathcal{M}\left(Pe\nabla p_0(x)\right). \tag{15}$$

We discuss the computational costs of evaluating this effective diffusion tensor and EVMFEM as an efficient alternative in Subsection 4.3.

3.2. Enhanced Velocity mixed FEM

We briefly discuss the EVMFEM scheme that is used in our adaptive numerical homogenization approach. EVMFEM has been applied successfully to a wide variety of complex multicomponent, multiphase flow and transport processes in porous medium including Equation of State (EOS), compositional flow [39]. In this section, we reiterate a semi-discrete variational formulation of the flow and transport problems using an EVMFEM domain decomposition approach [1]. This scheme enhances the trace of the discrete velocity space at the non-matching interface to construct a locally mass conservative $H(\mathrm{div},\Omega)$ conforming velocity approximation. The Enhanced Velocity space $\mathbf{V}_h^*$ is defined in [1] as,

$$\mathbf{V}_h^* = \bigoplus_{i=1}^{n}\mathbf{V}_{h,i}^0 \bigoplus \mathbf{V}_h^\Gamma \cap H(\mathrm{div};\Omega),$$

where $\mathbf{V}_{h,i}^0 = \{\mathbf{v}\in\mathbf{V}_{h,i} : \mathbf{v}\cdot\boldsymbol{\nu} = 0 \text{ on } \Gamma_i\}$ is the subspace of $\mathbf{V}_{h,i}$. We note that

$$\mathbf{V}_{h,i} = \{\mathbf{v}\in H(\mathrm{div};\Omega_i) : \mathbf{v}\Big|_T \in \mathbf{V}_h(T), \forall T\in\mathcal{T}_{h,i}\} \qquad i\in\{1,\ldots n\}$$

where $\mathcal{T}_{h,i}$ is a conforming, quasi-uniform and rectangular partition of Ω_i, $1\le i\le n$, with maximal element diameter h_i. At the non-matching interface, the virtual partitioning for subelements allows us to construct the fine-scale fluxes by considering additional basis functions in RT_0, as shown in Fig. 3.2. $\mathbf{V}_h^\Gamma$ is the span of all such basis functions defined on these sub-elements [1]. The pressure finite element approximation space on Ω is defined as,

$$W_h(\Omega) = \{w\in L^2(\Omega) : w\Big|_T \in W_h(T), \forall T\in\mathcal{T}_h\}. \tag{16}$$

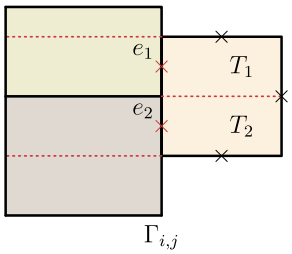

Fig. 3.2. Degrees of freedom for velocity and the Enhanced Velocity space at non-conforming interface $\Gamma_{i,j}$ between Ω_i and Ω_j.

For the flow problem, a weak solution of Eqns. (1)-(3) and Eqns. (7)-(8), is the pair $\mathbf{u}_h \in L^2\left(J, \mathbf{V}_h^*\right)$ and $p_h \in H^1\left(J, W_h\right)$ such that

$$\left(\mathbf{K}^{-1}\mathbf{u}_h, \mathbf{v}\right) - \left(p_h, \nabla \cdot \mathbf{v}_h\right) = -\langle g, \mathbf{v}_h \cdot \boldsymbol{\nu}\rangle_{\partial\Omega} \qquad \forall \mathbf{v}_h \in \mathbf{V}_h^*, \tag{17}$$

$$\left(\phi C_f \rho_{ref} \frac{\partial p_h}{\partial t}, w_h\right) + \left(\nabla \cdot (\rho(p_h)\mathbf{u}_h), w_h\right) = \left(f, w_h\right) \qquad \forall w_h \in W_h. \tag{18}$$

We also inherit the definition $\mathbf{V}_h^{*,0} \equiv \mathbf{V}_h^* \cap \{\mathbf{v} : \mathbf{v} \cdot \nu = 0 \text{ on } \partial\Omega\}$ for the transport problem from [1]. The semi-discrete variational formulation for the transport problem is: Given $\mathbf{u}_h \in L^2\left(J, \mathbf{V}_h^*\right)$ and $p_h \in H^1\left(J, W_h\right)$, find $\mathbf{d}_{i,h} \in L^2\left(J, \mathbf{V}_h^{*,0}\right)$ and $c_{i,h} \in H^1\left(J, W_h\right)$ such that,

$$\left(\frac{1}{\phi}\mathbf{D}_i^{-1}\mathbf{d}_{i,h}, \mathbf{v}_h\right) = \left(c_{i,h}, \nabla \cdot \mathbf{v}_h\right) \qquad \forall \mathbf{v}_h \in \mathbf{V}_h^{*,0}, \tag{19}$$

$$\begin{aligned}&\left(\phi C_f \rho_{ref} \frac{\partial p_h}{\partial t} c_{i,h}, w_h\right) + \left(\phi \rho(p_h) \frac{\partial c_{i,h}}{\partial t}, w_h\right) \\ &+ \left(\nabla \cdot (\rho(p_h)\mathbf{u}_h c_{i,h}), w_h\right) - \left(\nabla \cdot (\rho(p_h)\mathbf{d}_{i,h}), w_h\right) = \left(f, w_h\right) \qquad \forall w_h \in W_h.\end{aligned} \tag{20}$$

The EVMFEM ensures that both advective and diffusive fluxes are continuous at the subdomain interfaces resulting in local mass conservation. For single phase flow and species transport, the flow problem is inherently decoupled from the transport problem and therefore these two problems can be solved consecutively, as discussed above. A fully coupled formulation can also be described as: Find $\mathbf{u}_h \in L^2\left(J, \mathbf{V}_h^*\right)$, $p_h \in H^1\left(J, W_h\right)$, $\mathbf{d}_{i,h} \in L^2\left(J, \mathbf{V}_h^{*,0}\right)$, and $c_{i,h} \in H^1\left(J, W_h\right)$ such that, Eqns. (17) through (20) are satisfied. Fully coupled formulations have been applied for two-phase, black-oil, and EOS compositional flow in earlier works [1,39]. Further, a backward Euler scheme is used for temporal discretization resulting in a fully implicit system.

4. Adaptive homogenization

The adaptive homogenization approach presented here has two key steps: (1) numerical homogenization to obtain effective parameters (permeability, porosity etc.) at the coarse scale by solving local auxiliary problems, (2) use EVMFEM for AMR, with coarse and fine mesh regions identified using an adaptivity criterion, to solve coupled flow and transport problems. The subsections below describe the local numerical homogenization scheme, transient region identification using an indicator function, and the computational costs associated with effective dispersion tensor.

4.1. Local numerical homogenization

We first perform numerical homogenization to obtain coarse scale parameters for a given set of fine scale properties. To evaluate coarse scale parameters, we solve local auxiliary problems given by Eqn. (12) using fine scale parameters on a set of subdomains with periodic boundary conditions. The term local here is used to differentiate between a global periodic medium with a characteristic length scale, as opposed to a locally periodic or non-periodic medium. Fig. 4.1 depicts global and local periodicities in porous medium. Please note that this figure is only for the purpose of illustration and the shapes of the microstructures chosen are of no consequence. These local periodicities are often observed in well log data, where each layer represents a sedimentation and consolidation cycle.

The periodic porous medium is a convenient construct for mathematical analyses, however, such an assumption is not always valid for realistic subsurface problems. In our work, we consider highly heterogeneous flow parameters, where we relax these aforementioned assumptions. Fig. 4.2 shows a schematic of this local numerical homogenization where auxiliary problems are solved on a subdomain (Fig. 4.2, Ω_i, dotted red, left) at the fine scale. Each of these cell problems provides a coarse scale parameter on the coarse grid (Fig. 4.2, dotted red, right). These calculations are called offline, since they are performed as a pre-processing step once prior to the actual numerical simulations.

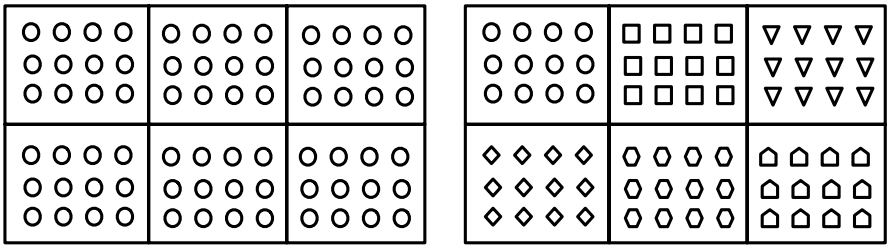

Fig. 4.1. Globally (left) and locally (right) periodic medium.

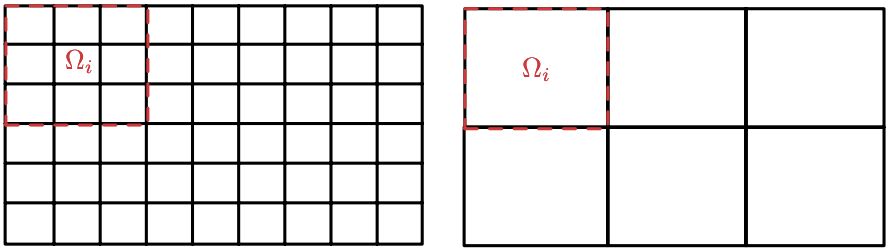

Fig. 4.2. Schematic of numerical homogenization to obtain coarse scale (right) parameters from fine scale (left). (For interpretation of the colors in the figure(s), the reader is referred to the web version of this article.)

4.2. Transient region identification and adaptivity criteria

The adaptive homogenization approach presented in this work uses coarse scale properties in the non-transient region identified using an indicator function. This indicator function (or adaptivity criteria) and details regarding transient and non-transient region demarcation are described here.

For multicomponent flow and transport in porous medium, the accuracy of the numerical solution depends upon how accurately the species concentration front is captured. In order to capture the front accurately, the fluid velocities must be resolved accurately along the front. This necessitates that a fine scale problem be solved, with fine scale properties for flow and transport, in the vicinity of the front for accuracy. The computational overheads are reduced by solving a coarse scale problem away from the transient region using coarse scale properties obtained from numerical homogenization. We therefore define a transient region in space, where the changes in species concentration are larger than a given threshold. This notion has also been used earlier by others [35] to reduce computational costs associated with different problems. In this work, we use the following adaptivity criteria to identify the transient region for spatial domain decomposition:

- Criterion 1

$$\Omega_f = \left\{\mathbf{x} : \max|c^n(\mathbf{x}) - c^n(\mathbf{y})| > \epsilon_{adap} \quad \forall \mathbf{y} \in \Omega_{neighbor}(\mathbf{x})\right\} \tag{21}$$

  We define $\Omega_{neighbor}(\mathbf{x}) = \{\mathbf{y} : \mathbf{y} \in E_j, |\partial E_i \cap \partial E_j| \neq \emptyset, \text{if } \mathbf{x} \in E_i\}$.
- Criterion 2

$$\Omega_f = \left\{\mathbf{x} : \text{ for } c^n(\mathbf{x}) \neq 0, \ \max|c^n(\mathbf{x}) - c^n(\mathbf{y})|/c^n(\mathbf{x}) > \epsilon_{adap} \quad \forall \mathbf{y} \in \Omega_{neighbor}(\mathbf{x})\right\} \tag{22}$$

In other words, the criterion 1 and 2 involves determining local maximum of differences in species concentrations in an absolute and relative sense.

Based upon these criteria, we divide the domain (Ω) into non-overlapping transient (Ω_f) and non-transient (Ω_c) subdomains, where flow and transport problems are solved at the fine and coarse scales, respectively. Fig. 4.3 shows a schematic of the domain decomposition approach used here. In what follows, coarse and non-transient, and fine and transient can be used interchangeably to refer to a subdomain. Further, the coarse and fine subdomain problems are coupled at the interface using the EVMFEM spatial discretization described earlier in section 3.2.

4.3. Species transport and dispersion

In this section, we describe the computational complexity of numerical homogenization associated with the flow and transport problems. We first discuss the computational costs of evaluating effective permeabilities for the coarse scale flow Eqn. (11). For the slightly compressible flow problem at hand, we solve d (spatial dimension) auxiliary problems defined by Eqn. (12) to obtain temporally invariant constants (effective permeability tensors). These invariants are computed and stored

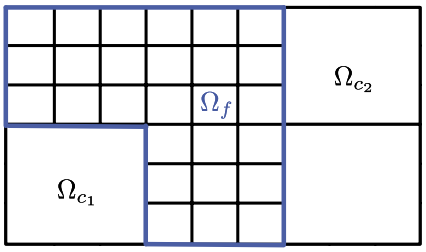

Fig. 4.3. Schematic of adaptive mesh refinement with coarse (Ω_c) and fine (Ω_f) domains.

once as a pre-processing step and later reused during simulation runtime as effective parameters for the coarse scale flow solve. The effective porosity is also an invariant and is trivially evaluated as a weighted arithmetic average of the fine scale values. The reduction in computational cost is evident, since these quantities need not be recalculated as the flow problem evolves in time.

We now consider the computational cost of evaluating macro-diffusivity tensor (Eqn. (15)) for the effective transport problem with advection and diffusion. As described in [12], effective parameters can be obtained by solving d and $d \times d$ auxiliary problems each for the first and second terms on the right hand side of Eqn. (15). The macro-diffusivities are temporally invariant only when the coarse scale velocities are also temporally invariant ($Pe\nabla p_0(x)$) and can therefore be pre-computed and stored for later use as before. However, for our practical problems of interest these coarse scale velocities can vary due to time varying boundary conditions and source/sink terms (q). For such cases, the effective macro-diffusivities must be recalculated at every time-interval. This is true even for compressible flow problems, where velocities can vary with time even in the absence of time varying boundary conditions and source/sink terms. The re-evaluation of these effective macro-diffusivities, therefore, becomes computationally expensive compared to solving the original fine scale problem directly.

In order to avoid these issues, we are using the EVMFEM domain decomposition approach to solve the fine scale problem in the vicinity of the species concentration front (or subdomains where gradient of concentration is large) coupled to a coarse scale problem away from this front, where gradient of species concentration is small. In addition, realistic porous media are highly heterogeneous and an adaptive mesh refinement using the EVMFEM domain decomposition allows us to circumvent the scale separation and periodic medium assumptions of the formal two-scale homogenization theory.

Further, the derivation of effective macroscale equations in [12] relies upon an assumption of high Peclet numbers or in other words ε order diffusion. This results in restriction on the choice of coarse subdomains so as to preserve this assumption. A local mesh refinement in the vicinity of the species concentration front also allows us to relax this restriction on the choice of coarse subdomains. We note that for realistic porous media, local Peclect numbers (high, moderate, or low) vary spatially and are dictated by the heterogeneous property distributions. In the later sections, we present numerical experiments on Gaussian, channelized and heterogeneous permeability distributions using this adaptive homogenization approach that are in good agreement with fine scale solutions for a wide range of Peclet numbers.

4.4. Solution algorithm

This subsection describes the solution algorithm for the adaptive homogenization approach discussed above. The unit-cell (auxiliary) problems are solved (assuming local periodicity) as a pre-processing step to evaluate coarse scale coefficients using numerical homogenization. This step can be carried out in parallel to further improve computational efficiency, since the unit-cell problems are mutually independent. We refer to this calculation as the offline stage because the parameters (permeability, porosity, etc.) remain temporally invariant.

We obtain a non-linear system of equations from the fully discrete (space and time) formulation of the flow and transport PDEs. A Newton method is then applied to this non-linear system of equations to obtain a linear algebraic system of equations that can be solved using an appropriate linear solver. Algorithm 1 shows a brief outline of the solution algorithm. We note that n and k are the time and non-linear iteration counter, t_n and t_{n+1} are the current and next time, Δt current time-step size, T the final time, $max(\vec{R}_{nl})$ the max norm of the non-linear residual vector, and ϵ_{nl} the non-linear tolerance. At each time iterate, we evaluate the adaptivity criteria (Eqn. (21) or (22)); at the coarse scale, to identify the transient region and perform a domain decomposition into fine (Ω_f) and coarse Ω_c subdomains. A projection/reconstruction operation is performed if the identifier changes from coarse to fine or vice versa, respectively. Note that we only consider semi-structured, nested grids as shown in Fig. 4.2. The reconstruction is performed by simply using previous time step unknowns (p, c) and since these are intensive properties the operation remains mass conservative. In other words, coarse grid values from the previous time-step (n) are used to initialize the fine grid computation for the next time-step ($n+1$) such that, for given $q_H \in W_h(\Omega_c)$,

Algorithm 1: Adaptive multi-scale solution algorithm for the coupled flow and transport problem.

Solve unit-cell problems, Eqns. (12), on subdomains (Ω_i) using fine scale parameters to obtain coarse scale parameters for the entire domain ($\Omega = \cup\Omega_i$, see Fig. 4.1).
while $t_n \leq T$ **do**
  Identify transient (Ω_f) region using adaptivity criteria (Eqn. (21) or (22)) and p, c at t_n ($\Omega_f \cup \Omega_c = \Omega$).
  Mass conservative initialization of primary unknowns:

  1. Reconstruct primary unknowns $p^{n+1,0}, c^{n+1,0}$ for the fine scale transient region (Ω_f).
  2. Project primary unknowns $p^{n+1,0}, c^{n+1,0}$ for the coarse scale non-transient region (Ω_c).

  while $max(\vec{R}_{nl}) > \epsilon_{nl}$ **do**

    1. Use fine and coarse scale parameters in the transient (Ω_f) and non-transient (Ω_c) regions, respectively.
    2. Use enhanced velocity (EV) scheme to couple coarse and fine subdomains.
    3. Solve linear algebraic system for the coupled flow and transport problem to obtain a Newton update $p^{n+1,k+1}$, $c^{n+1,k+1}$.

  end
  $t_{n+1} = t_n + \Delta t$, $n := n + 1$
end

$$q_h^{n+1,0} := q_H^n\Big|_{T_j} \qquad T_j \subset T,\ j \in \{1, ..m\}. \tag{23}$$

Here, $T_j \in \mathcal{T}_h^{n+1}(\Omega_f)$ and $T \in \mathcal{T}_h^n(\Omega_c)$.

On the other hand, a mass conservative projection (L^2-projection) is used for coarsening which reduces to a simple arithmetic average of fine scale unknowns (p, c) for an incompressible flow problems. In other words, for given $q_h \in W_h(\Omega_f)$, the L^2-projection is defined by

$$(q_h - P_H q_h, w) = 0 \quad \forall w \in W_H(\Omega_c). \tag{24}$$

We set $q_h^{n+1,0} := P_H q_h^n$. We note that the projection and reconstruction operations on q_h can be applied to pressure (p_h) and concentration (c_h) unknowns. This is followed by a non-linear solve of the system of algebraic equations resulting from the spatial and temporal discretization after domain decomposition. The non-linear iterations are performed until the max norm satisfies a desired tolerance corresponding to the error in phase and component mass conservation equations. Significant computational savings are obtained for time dependent problems since the effective values of porosity and permeability are only evaluated once for a given fine scale distribution.

5. Numerical results

Three numerical experiments are presented to demonstrate our proposed adaptive numerical homogenization approach. The first numerical example is a comparison between adaptive and fine scale simulations for homogeneous property distribution. This is followed by similar comparisons for heterogeneous porous media with two different property distributions, namely: Gaussian and channelized permeability. The heterogeneous permeabilities were obtained from SPE10 dataset [36]: (1) layer 20 and (2) layer 37.

The reservoir domain is 110 ft × 30 ft (33 m × 9 m) with fine scale permeability distribution available for a 220×60 grid with grid block size 0.5 ft×0.5 ft (0.15 m × 0.15 m). A coarse scale permeability distribution for a 22×6 grid is obtained using two-scale homogenization, as a preprocessing step at the beginning of the simulation, with grid block size of 5 ft × 5 ft (1.5 m × 1.5 m). Here a local cell problem, for a 10 × 10 grid, with periodic boundary conditions is solved at the fine scale.

A rate specified injection well and a pressure specified production well are located at the bottom left and top right corner, respectively. The production pressure is specified at 1000 psi (6.89×10^6 Pa) with a continuous species injection of $\hat{c} = 1$. The initial reservoir pressure and species concentrations are taken to be 1000 psi (6.89×10^6 Pa) and zero, respectively. Further, the fluid compressibility, density, and viscosity are assumed to be 1×10^{-6} psi^{-1} (1.45×10^{-10} Pa^{-1}), 66.5 lb/ft^3 (1065.228 kg/m^3), and 1 cP (0.001 Pa · s), respectively. Further, we define the computed Peclet number as,

$$Pe_k = \frac{|u_k| l}{D_0}. \tag{25}$$

Here, u_k is the velocity in k direction, l is the fine scale length (0.5 ft (0.15 m)), and D_0 is the fine scale, diffusion/dispersion coefficient (0.001 ft^2/day (9.3×10^{-4} m^2/day)). All simulations are performed for a total duration of 200 days with a no-flow external boundary condition unless explicitly stated otherwise in the subsections below. The timestep size is chosen to be 1 day for all the numerical experiments. Although porosity distributions are not shown, the coarse scale porosities were obtained from the fine scale SPE10 dataset by using a volume weighted arithmetic average.

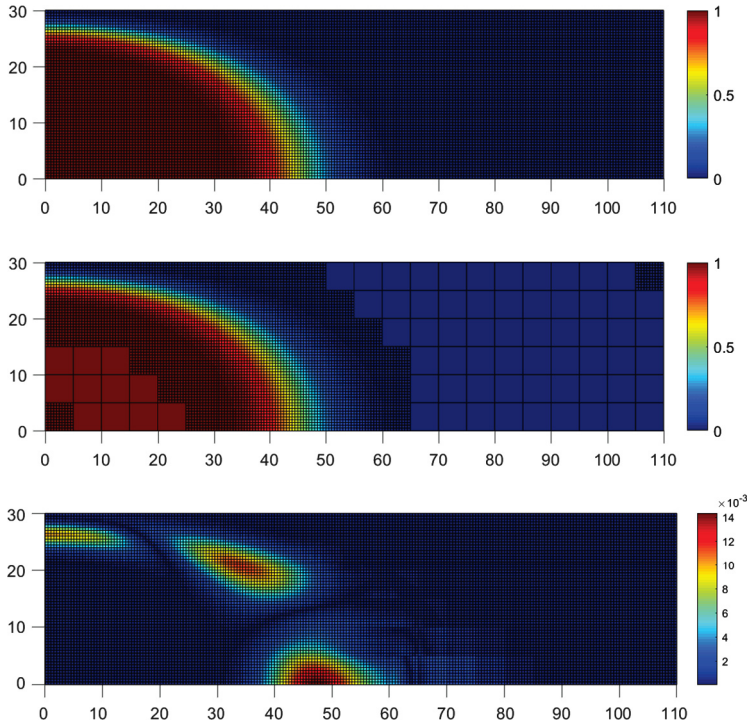

Fig. 5.1. Concentration profiles at 50 days for fine (top), adaptive (middle) approaches and difference (bottom) in homogeneous permeability and porosity.

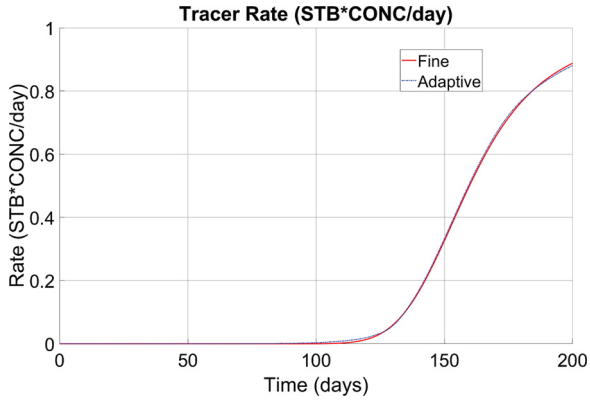

Fig. 5.2. Species concentration history at the production well for the homogeneous permeability distribution.

5.1. Homogeneous case

A homogeneous and isotropic permeability distribution is assumed using a diagonal permeability tensor of 50 mD and porosity of 0.1. The injection rate is taken to be 2 STB/day (10.87×10^5 m^3/s). Fig. 5.1 shows the spatial distribution of the species concentrations after 50 days for the fine (top), adaptive (middle) simulations and difference (bottom). The difference between adaptive and fine scale solutions, Fig. 5.1 (bottom), uses reconstructed species concentration for the coarse subdomains of the adaptive grids.

Fig. 5.2 shows the species concentration history at the production well after 200 days. The fine and adaptive results are in excellent agreement. Since the fine scale permeability distribution is homogeneous the homogenized or coarse scale distribution is also spatially invariant at 50 mD (49.3462×10^{-15} m^2).

5.2. Gaussian permeability distribution

For this numerical test, we chose a near Gaussian permeability distribution as shown in Fig. 5.3 (top) from layer 20 of SPE10 dataset. The coarse scale permeability, Fig. 5.3 (bottom), distribution and coarse scale porosity was evaluated using numerical homogenization. The injection rate was assumed to be 3 STB/day (16.30×10^5 m^3/s).

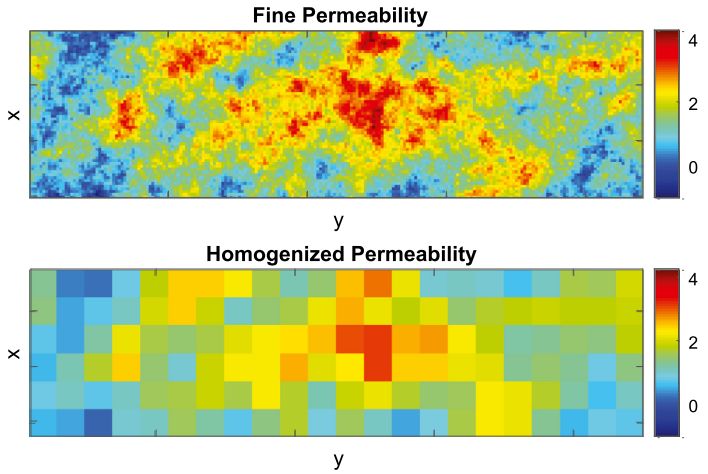

Fig. 5.3. Fine and coarse scale permeability distributions in log scale for SPE 10 layer 20.

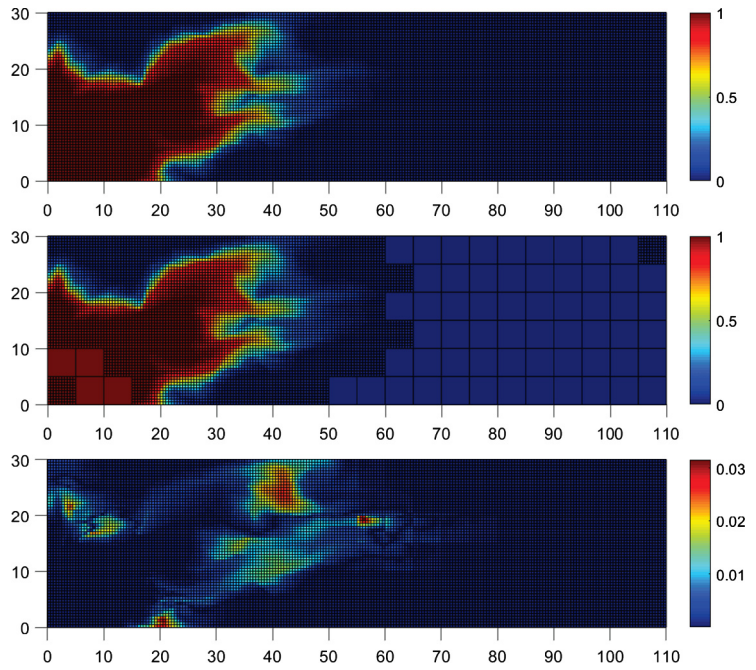

Fig. 5.4. Concentration profiles at 50 days for fine (top) and adaptive (middle) approaches and the difference (bottom) between them.

Figs. 5.4 (top and middle) shows the concentration profiles after 50 days for fine scale and adaptive homogenization approaches. Fig. 5.4 (bottom) gives the difference between adaptive and fine scale solutions that uses reconstructed species concentration for the coarse subdomains of the adaptive grids. Fig. 5.5 shows the species concentration history at the production well after 200 days. The results show that the concentrations using adaptive homogenization approaches are in good agreement with the fine scale solution.

Fig. 5.6 shows the species concentration histories comparing fine and adaptive simulation for different injection rates of 1 STB/day (5.43×10^5 m^3/s), 5 STB/day (27.17×10^5 m^3/s) and 10 STB/day (54.34×10^5 m^3/s). Please note that for heterogeneous permeability distributions we obtain a range of Peclet numbers by changing the injection rates. We label the species concentration histories with $Pe1$, $Pe2$, and $Pe3$ corresponding to 1 STB/day (5.43×10^5 m^3/s), 5 STB/day (27.17×10^5 m^3/s) and 10 STB/day (54.34×10^5 m^3/s), such that the average Peclet numbers satisfy $Pe1 < Pe2 < Pe3$. Table 1 shows the range of Peclet numbers obtained for each of these injection rates. The species concentration histories for the fine and adaptive simulations are in good agreement for the three cases.

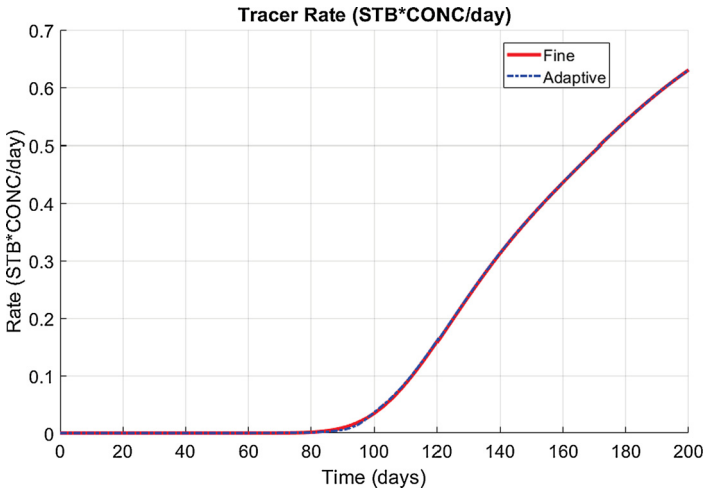

Fig. 5.5. Species concentration history at the production well for SPE 10 layer 20.

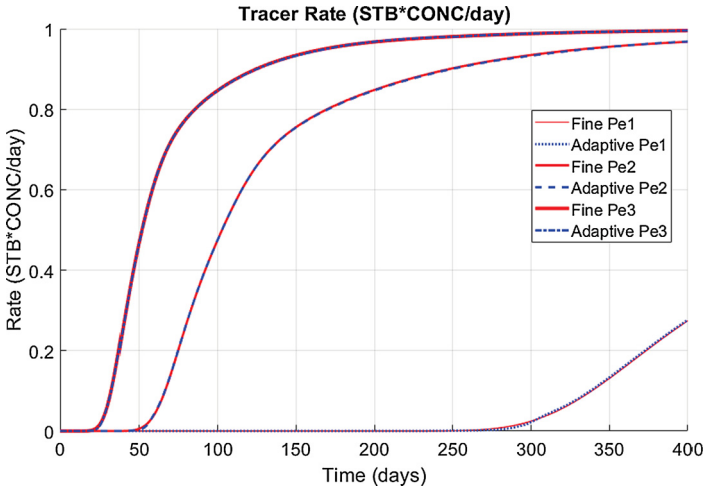

Fig. 5.6. Different Pe numbers species production history for fine and adaptive methods.

Table 1
Range of Peclet numbers for SPE 10 layer 20.

q_{inj}	Pe_x	Pe_y	
1	3.3×10^{-4}	3.8×10^{-3}	Min
1	6.5×10^{2}	4.0×10^{2}	Max
5	1.7×10^{-3}	1.8×10^{-2}	Min
5	3.2×10^{3}	2.0×10^{3}	Max
10	3.3×10^{-3}	3.8×10^{-2}	Min
10	6.5×10^{3}	4.0×10^{3}	Max

5.3. Channelized permeability distribution

Here we choose the permeability distribution from layer 37 of the SPE10 dataset. The coarse scale permeabilities, Fig. 5.7 (bottom), are again evaluated using local numerical homogenization. It is important to note that the channel connectivity is lost in the homogenized coarse scale permeabilities. Our proposed approach recovers this connectivity by solving a fine scale problem in the transient region.

Figs. 5.8 (top and middle) shows the concentration profile after 50 days for fine scale and adaptive homogenization approaches. Fig. 5.8 (bottom) gives the difference between adaptive and fine scale solutions that uses reconstructed species concentration for the coarse subdomains of the adaptive grids. These results indicate that even for highly channelized permeability distributions our proposed approach is able to accurately capture the species concentration front.

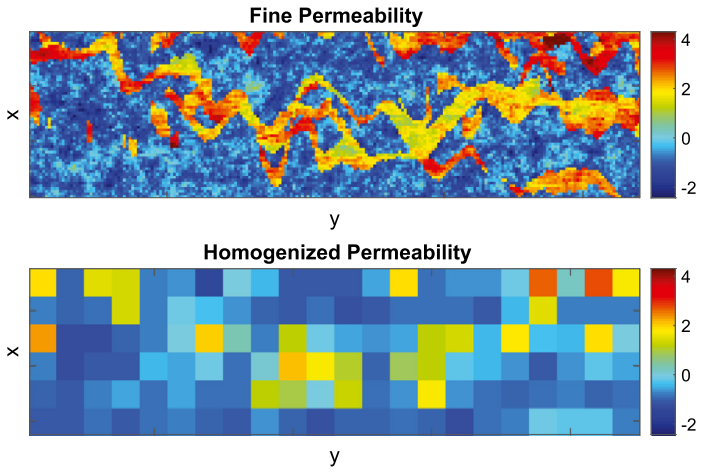

Fig. 5.7. Fine and coarse scale permeability distributions in log scale for SPE 10 layer 37.

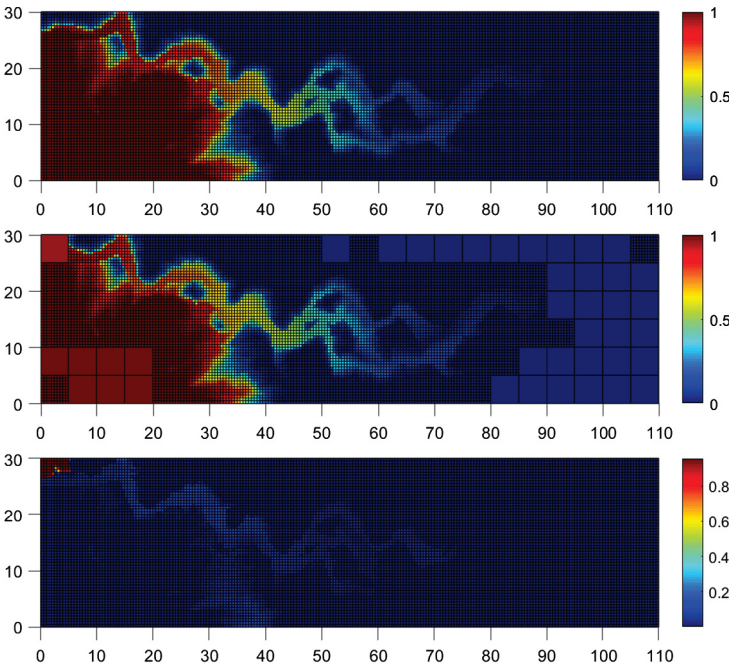

Fig. 5.8. Concentration profiles at 50 days for fine (top), adaptive (middle) approaches and difference (bottom).

Fig. 5.9 shows that species concentration history at the production well after 200 days for the fine and adaptive cases are in good agreement.

Similar to the Gaussian permeability distribution, Fig. 5.10 shows the species concentration histories comparing fine and adaptive simulation for different injection rates of 2 STB/day (10.87×10^5 m^3/s), 5 STB/day (27.17×10^5 m^3/s) and 10 STB/day (54.34×10^5 m^3/s). Again, a heterogeneous permeability distributions results in a range of Peclet numbers for different injection rates. The species concentration histories are labeled as $Pe1$, $Pe2$, and $Pe3$ corresponding to 2 STB/day (10.87×10^5 m^3/s), 5 STB/day (27.17×10^5 m^3/s and 10 STB/day (54.34×10^5 m^3/s), such that the average Peclet numbers satisfy $Pe1 < Pe2 < Pe3$, as before. Table 2 shows the range of Peclet numbers obtained for each of these injection rates. Again, the species concentration histories for the fine and adaptive simulations are in good agreement for the three cases.

5.4. Effect of adaptivity criteria and tolerance

We present a sensitivity analysis for the choice of tolerance on the two adaptivity criteria and the resulting changes in computational speedup and solution accuracy. We define the relative error in a domain Ω at time t as follows,

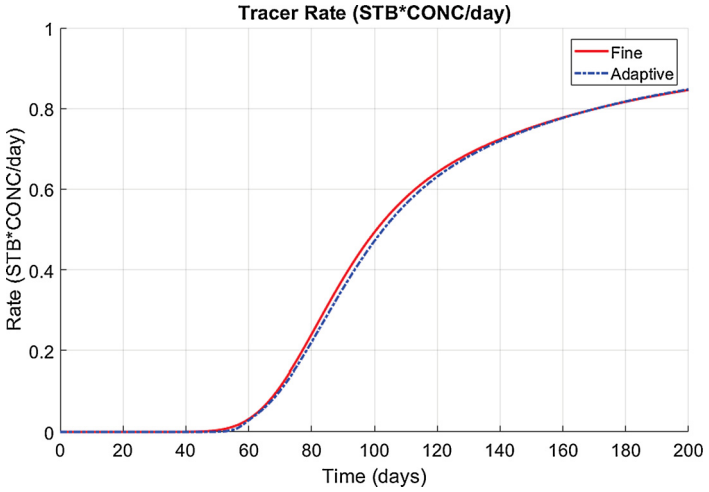

Fig. 5.9. Species concentration history at the production well for SPE layer 37.

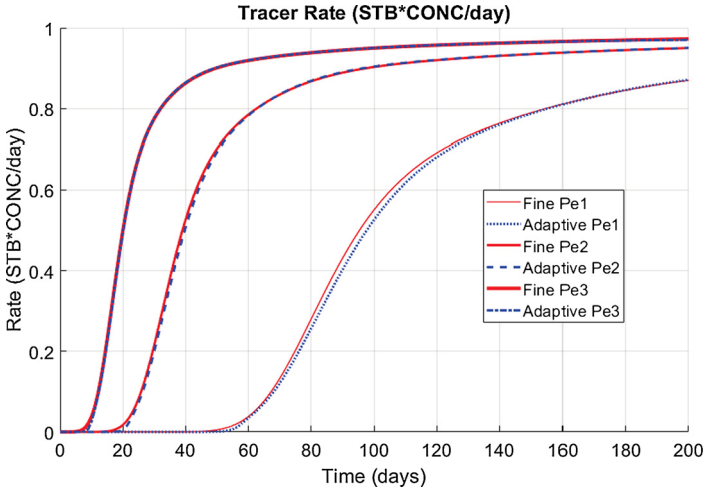

Fig. 5.10. Different Pe numbers species production history for fine and adaptive methods.

Table 2
Range of Peclet numbers for SPE 10 layer 37.

q_{inj}	Pe_x	Pe_y	
2	3.8×10^{-6}	1.4×10^{-6}	Min
2	1.9×10^{3}	1.6×10^{3}	Max
5	9.4×10^{-6}	3.5×10^{-6}	Min
5	4.9×10^{3}	4.0×10^{3}	Max
10	1.8×10^{-5}	6.9×10^{-6}	Min
10	9.8×10^{3}	8.1×10^{3}	Max

$$e_{c,\Omega} = \frac{\left\| c_f(\cdot,t) - c_{adapt}(\cdot,t) \right\|_{l^2}}{\left\| c_f(\cdot,t) \right\|_{l^2}} \tag{26}$$

where c_f is the fine scale concentration solution obtained from fine scale discretization, c_{adapt} is the solution obtained using adaptive numerical homogenization. We define a different relative error at the production well for the time interval $(0, T]$ as follows,

$$\tilde{e}_{c,\Omega} = \frac{\left\| c_f(\tilde{x},\cdot) - c_{adapt}(\tilde{x},\cdot) \right\|_{l^2}}{\left\| c_f(\tilde{x},\cdot) \right\|_{l^2}} \tag{27}$$

Table 3
Errors for entire domain $e_{c,\Omega}$ and tolerance for the Gaussian permeability case.

ϵ_{adapt}	Criterion 1		Criterion 2	
	Speedup	$e_{c,\Omega}$	Speedup	$e_{c,\Omega}$
0.4	≈ 12	0.1716	≈ 3	0.1092
0.3	≈ 5	0.1256	≈ 3	0.0838
0.2	≈ 3	0.0855	≈ 2	0.0579
0.1	≈ 2	0.0321	≈ 2	0.0309
0.05	≈ 2	0.0271	≈ 2	0.0266

Table 4
Errors at Production well $\tilde{e}_c$ and tolerance for the Gaussian permeability case.

ϵ_{adapt}	Criterion 1		Criterion 2	
	Speedup	$\tilde{e}_c$	Speedup	$\tilde{e}_c$
0.4	≈ 12	0.1329	≈ 3	0.0434
0.3	≈ 5	0.1090	≈ 3	0.0265
0.2	≈ 3	0.0827	≈ 2	0.0228
0.1	≈ 2	0.0311	≈ 2	0.0184
0.05	≈ 2	0.0166	≈ 2	0.0168

Table 5
Errors for entire domain $e_{c,\Omega}$ and tolerance at $T = 200$ day for the Channelized permeability case.

ϵ_{adapt}	Criterion 1		Criterion 2	
	Speedup	$e_{c,\Omega}$	Speedup	$e_{c,\Omega}$
0.4	≈ 10	0.3967	≈ 3	0.1556
0.3	≈ 4	0.2746	≈ 3	0.0838
0.2	≈ 3	0.1002	≈ 3	0.0583
0.1	≈ 2	0.0668	≈ 2	0.0523
0.05	≈ 2	0.0510	≈ 2	0.0510

Table 6
Errors at Production well $\tilde{e}_c$ and tolerance for the Channelized permeability case.

ϵ_{adapt}	Criterion 1		Criterion 2	
	Speedup	$\tilde{e}_c$	Speedup	$\tilde{e}_c$
0.4	≈ 10	0.3207	≈ 3	0.0448
0.3	≈ 4	0.2204	≈ 3	0.0334
0.2	≈ 3	0.1336	≈ 3	0.0266
0.1	≈ 2	0.0612	≈ 2	0.0279
0.05	≈ 2	0.0268	≈ 2	0.0286

where $\tilde{x}$ is the production well location, $t \in (0, T]$. The computational speedup is defined as the ratio of CPU times for the fine scale simulation to the adaptive simulation.

As shown in Tables 3–6, this sensitivity analysis suggests that Criterion 2 is weakly related to the choice of tolerance ϵ_{adap} compared to criterion 1 for a desired solution accuracy. On the other hand, Criterion 1 results in substantial computational speedups if a lower solution accuracy is required. We present two different error calculations $e_{c,\Omega}$ and $\tilde{e}_{c,\Omega}$ one for the entire computational domain at the final time and another for the production well over the entire time interval, respectively. However, for subsurface porous media applications the second error calculation is considered practically more relevant. Furthermore, engineering applications and planning often require evaluation of a large number of scenarios such as well placement, injection and production schedules with a lower emphasis on the requirement of desired accuracy. For such cases, our adaptive numerical homogenization approach provides additional computational speedups when the accuracy requirements are not high. A break-even or optimal threshold can only be strictly determined if the fine scale solution is known beforehand which is seldom the case. Our sensitivity analysis shows that we obtain a speedup of at least 2 times for a very tight tolerance on adaptivity criteria for an accurate solution.

6. Conclusions

We developed a locally mass conservative, adaptive multiscale method by combining local numerical homogenization and EVMFEM domain decomposition for flow and transport problems in heterogeneous porous media. Our proposed approach was compared against fine scale solution using benchmark SPE10 datasets. The results are in excellent agreement for both

Gaussian and channelized permeability distributions due to accurate identification of the species concentration fronts (or the transient zones). The adaptive homogenization approach relaxes the scale separation and periodicity assumptions of the two-scale homogenization theory allowing flexibility in the treatment of realistic porous media. The adaptivity captures the effects of dispersion irrespective of the Peclet numbers that can vary by orders of magnitude. Since the scale separation assumption is relaxed, the choice of REV is not restrictive. Specifically, for channelized permeabilities we do not require REV to be restricted by the channel width to preserve connectivity.

Furthermore, a brief sensitivity study on the choice of tolerance for the adaptivity criteria is also presented. We note that the solution accuracy can be further increased by using stricter tolerances for the two adaptivity criteria. Extensions to general multiphase flow and transport problems with appropriate error estimators as better adaptivity criteria will be presented in future works.

Acknowledgements

This work was supported by DOE, Center for Frontiers of Subsurface Energy Security (CFSES) grant DE-SC000111; NSF, BIGDATA: Collaborative Research Award 1546553. We would also like to thank our Center for Subsurface Modeling Industrial affiliates for their continued support. First author would like to acknowledge support of the Faculty Development Competitive Research Grant (Grant No. 110119FD4502), Nazarbayev University.

Appendix A. Supplementary material

Supplementary material related to this article can be found online at https://doi.org/10.1016/j.jcp.2019.02.014.

References

[1] J.A. Wheeler, M.F. Wheeler, I. Yotov, Enhanced velocity mixed finite element methods for flow in multiblock domains, Comput. Geosci. 6 (3–4) (2002) 315–332.
[2] C. Farmer, Upscaling: a review, Int. J. Numer. Methods Fluids 40 (1–2) (2002) 63–78.
[3] T. Arbogast, Mixed multiscale methods for heterogeneous elliptic problems, in: I.G. Graham, T.Y. Hou, O. Lakkis, R. Scheichl (Eds.), Numerical Analysis of Multiscale Problems, in: Lecture Notes in Computational Science and Engineering, vol. 83, Springer, Berlin, Heidelberg, 2012, pp. 243–283.
[4] T. Arbogast, Implementation of a locally conservative numerical subgrid upscaling scheme for two-phase Darcy flow, Comput. Geosci. 6 (3–4) (2002) 453–481.
[5] T. Arbogast, S.E. Minkoff, P.T. Keenan, An Operator-Based Approach to Upscaling the Pressure Equation, vol. 23, WIT Press, 1998.
[6] L.J. Durlofsky, Upscaling of geocellular models for reservoir flow simulation: a review of recent progress, in: 7th International Forum on Reservoir Simulation Bühl/Baden-Baden, Germany, 2003, pp. 23–27.
[7] X.-H. Wu, Y. Efendiev, T.Y. Hou, Analysis of upscaling absolute permeability, Discrete Contin. Dyn. Syst., Ser. B 2 (2) (2002) 185–204.
[8] G. Allaire, Homogenization and two-scale convergence, SIAM J. Math. Anal. 23 (6) (1992) 1482–1518.
[9] A. Mikelić, V. Devigne, C. Van Duijn, Rigorous upscaling of the reactive flow through a pore, under dominant Peclet and Damkohler numbers, SIAM J. Math. Anal. 38 (4) (2006) 1262–1287.
[10] V.V. Jikov, S.M. Kozlov, O.A. Oleinik, Homogenization of Differential Operators and Integral Functionals, Springer Science & Business Media, 2012.
[11] A. Bensoussan, J.-L. Lions, G. Papanicolaou, Asymptotic Analysis for Periodic Structures, vol. 5, North-Holland Publishing Company, Amsterdam, 1978.
[12] B. Amaziane, A. Bourgeat, M. Jurak, Effective macrodiffusion in solute transport through heterogeneous porous media, Multiscale Model. Simul. 5 (1) (2006) 184–204.
[13] A. Mikelić, Homogenization of nonstationary Navier-Stokes equations in a domain with a grained boundary, Ann. Mat. Pura Appl. 158 (1) (1991) 167–179.
[14] G. Allaire, Homogenization of the Stokes flow in a connected porous medium, Asymptot. Anal. 2 (3) (1989) 203–222.
[15] I. Babuška, J.E. Osborn, Generalized finite element methods: their performance and their relation to mixed methods, SIAM J. Numer. Anal. 20 (3) (1983) 510–536.
[16] T.Y. Hou, X.-H. Wu, A multiscale finite element method for elliptic problems in composite materials and porous media, J. Comput. Phys. 134 (1) (1997) 169–189.
[17] Y. Efendiev, T.Y. Hou, Multiscale Finite Element Methods: Theory and Applications, vol. 4, Springer Science & Business Media, 2009.
[18] Y. Efendiev, J. Galvis, T.Y. Hou, Generalized multiscale finite element methods (gmsfem), J. Comput. Phys. 251 (2013) 116–135.
[19] P. Jenny, S.H. Lee, H.A. Tchelepi, Adaptive multiscale finite-volume method for multiphase flow and transport in porous media, Multiscale Model. Simul. 3 (1) (2005) 50–64.
[20] I. Lunati, P. Jenny, Multiscale finite-volume method for compressible multiphase flow in porous media, J. Comput. Phys. 216 (2) (2006) 616–636.
[21] S.H. Lee, H. Zhou, H.A. Tchelepi, Adaptive multiscale finite-volume method for nonlinear multiphase transport in heterogeneous formations, J. Comput. Phys. 228 (24) (2009) 9036–9058.
[22] D.A. Barajas-Solano, A.M. Tartakovsky, Hybrid multiscale finite volume method for advection-diffusion equations subject to heterogeneous reactive boundary conditions, Multiscale Model. Simul. 14 (4) (2016) 1341–1376.
[23] T.J. Hughes, G.R. Feijóo, L. Mazzei, J.-B. Quincy, The variational multiscale method—a paradigm for computational mechanics, Comput. Methods Appl. Mech. Eng. 166 (1–2) (1998) 3–24.
[24] T. Arbogast, S.L. Bryant, Numerical subgrid upscaling for waterflood simulations, in: SPE Reservoir Simulation Symposium, Society of Petroleum Engineers, 2001.
[25] E. Weinan, B. Engquist, The heterogenous multiscale methods, Commun. Math. Sci. 1 (1) (2003) 87–132.
[26] A. Abdulle, W. E, B. Engquist, E. Vanden-Eijnden, The heterogeneous multiscale method, Acta Numer. 21 (2012) 1–87.
[27] E. Weinan, B. Engquist, X. Li, W. Ren, E. Vanden-Eijnden, Heterogeneous multiscale methods: a review, Commun. Comput. Phys. 2 (3) (2007) 367–450.
[28] T. Arbogast, G. Pencheva, M.F. Wheeler, I. Yotov, A multiscale mortar mixed finite element method, Multiscale Model. Simul. 6 (1) (2007) 319–346.
[29] V. Girault, D. Vassilev, I. Yotov, Mortar multiscale finite element methods for Stokes–Darcy flows, Numer. Math. 127 (1) (2014) 93–165.
[30] M.T. Balhoff, S.G. Thomas, M.F. Wheeler, Mortar coupling and upscaling of pore-scale models, Comput. Geosci. 12 (1) (2008) 15–27.
[31] B. Ganis, I. Yotov, Implementation of a mortar mixed finite element method using a multiscale flux basis, Comput. Methods Appl. Mech. Eng. 198 (49) (2009) 3989–3998.

[32] M. Peszynska, Q. Lu, M.F. Wheeler, Coupling different numerical algorithms for two phase fluid flow, in: J. Whiteman (Ed.), Proceedings of Mathematics of Finite Elements and Applications, Brunel University, Uxbridge, UK, 1999, pp. 205–214.
[33] M. Peszyńska, M.F. Wheeler, I. Yotov, Mortar upscaling for multiphase flow in porous media, Comput. Geosci. 6 (1) (2002) 73–100.
[34] E. Chung, Y. Efendiev, T.Y. Hou, Adaptive multiscale model reduction with generalized multiscale finite element methods, J. Comput. Phys. 320 (2016) 69–95.
[35] J.E. Aarnes, Y. Efendiev, An adaptive multiscale method for simulation of fluid flow in heterogeneous porous media, Multiscale Model. Simul. 5 (3) (2006) 918–939.
[36] M.A. Christie, M.J. Blunt, Tenth SPE comparative solution project: a comparison of upscaling techniques, SPE Reserv. Eval. Eng. 4 (04) (2001).
[37] D.W. Peaceman, Interpretation of well-block pressures in numerical reservoir simulation with nonsquare grid blocks and anisotropic permeability, Soc. Pet. Eng. J. 23 (03) (1983) 531–543.
[38] G.A. Pavliotis, A. Stuart, Multiscale Methods: Averaging and Homogenization, Springer Science & Business Media, 2008.
[39] S.G. Thomas, M.F. Wheeler, Enhanced velocity mixed finite element methods for modeling coupled flow and transport on non-matching multiblock grids, Comput. Geosci. 15 (4) (2011) 605–625.